Synthesis and Characterization of Nanocapsules with Shells Made up of Al_{13} Tridecamers

Xim Bokhimi,*,† Enrique Lima,‡ and Jaime Valente§

Institute of Physics, The National University of Mexico (UNAM), A.P. 20-364, 01000 México D. F., Mexico, Universidad Autónoma Metropolitana-Iztapalapa, A.P. 55-532, 09340 México D. F., Mexico, and Instituto Mexicano del Petróleo, A.P. 140-805, 07730 México D. F., Mexico

Received: July 8, 2005; In Final Form: September 8, 2005

The synthesis of samples by the sol−gel method with aluminum tri-*sec*-butoxide as cation precursor, 2-propanol as solvent, and sulfuric acid as hydrolysis catalyst gave rise to nanocapsules with an average diameter of 20 nm and a shell thickness of 3.5 nm. The analysis of the X-ray diffraction patterns and the ^{27}Al MAS NMR spectra showed that the shell of the nanocapsules was made up of Al_{13} tridecamers ordered in a noncrystalline symmetry. The interaction between the capsule's shells opened the capsule structure, producing curved fibers, but maintaining the atomic local order. This opening of the capsules favored the reordering of the atomic local order of Al_{13} tridecamers into the one of crystalline boehmite, when the sample was aged at room temperature for several days; it also increased the pore volume and the specific surface area of the sample. The crystallization transformed the curved fibers into rods made of small crystalline boehmite bars. The capsule morphology was preserved after calcining the nonaged sample at 700 °C, indicating that the transformation of the phase made up of ordered Al_{13} tridecamers into a noncrystalline alumina was pseudomorphic. We describe and partially explain one of the possible atomic ordering evolutions from the one of an isolated Al_{13} tridecamer, to the phase forming the nanocapsules shell, until eventually coming to the ordering corresponding to boehmite crystalline rods.

Introduction

Transition aluminas are generally produced industrially by precipitation, drying, and calcining of aluminum oxy-hydroxides. These oxides have been widely used as absorbents, ceramics, composite materials, catalysts, and particularly as catalyst supports in several chemical processes, mainly due to their low cost, high specific surface area, surface acidity, and the important interaction that they exhibit with deposited transition metals.[1−4]

The catalytic properties of aluminas largely depend on the crystalline structure and texture. The textural parameters of alumina, such as specific surface area, pore size, and shape, determine some of the technological properties of the catalyst, for example, bed volume, accessibility of reactants, and product retention.[4−10]

A specific alumina texture depends on the corresponding texture of the sample with the alumina precursor phase. Of pecial interest is the case where the transformation of the precursor phase into alumina is pseudomorphic, because it does not change the precursor's sample texture, for example, when alumina is prepared from boehmite, one of its main precursors,[11,12] which can crystallize into thin plates[13,14] or into thin rods.[15−21]

This alumina precursor can be synthesized with different techniques that allow control of its texture:[21−23] crystallite size, pore diameter, and morphology, pore volume, and specific surface area. Pore diameter and pore morphology can be changed by using chemical templates in the synthesis,[15,24] while crystallite size can be controlled by performing the synthesis under hydrothermal conditions at different temperatures;[21,25−27] when crystallites are plates, their size decreases as the synthesis temperature decreases,[26,27] and when they are rods the particle aspect ratio decreases as this temperature increases.[25]

When boehmite crystallizes as thin flat plates, the largest crystallite surface is perpendicular to the [010] direction, which produces a very broad (020) reflection in the X-ray diffraction pattern and relatively sharp peaks corresponding to the (200) and (002) planes.[28] The extreme case corresponds to a plate thickness of only one unit cell observed in samples prepared at room temperature. There are reports, however, where the X-ray diffraction pattern of the sample does not have the (020) reflection, which can be interpreted as a lack of order in the atomic distribution along the *b* axis.[28,29] The X-ray diffraction pattern of the boehmite samples prepared at room temperature by the sol−gel technique also contains diffraction peaks than can be neither associated to boehmite[28−30] nor to the starting materials used in the synthesis; they, however, could belong to intermediate components generated before the formation of the boehmite crystalline structure.

In the literature about the synthesis of boehmite the appearance of any precursor of this phase at room temperature is not reported. The only interesting topic related to this point is the fact that in the solutions of the salts used to synthesize boehmite, for example aluminum nitrate, Al−O polynuclear cations are generated. From them, only one, the polycation Al_{13} tridecamer, $[Al_{13}O_4(OH)_{24}(H_2O)_{12}]^{7+}$, has been well determined: it is made of one Al−O tetrahedron at tridecamer's center, surrounded by twelve Al−O octahedra,[31] forming a Keggin structure.[32] The clustering and partial breakdown of this tridecamer, by aging samples at 90 °C, results in the formation of gibbsite.[33] Tridecamers with the Keggin structure also exist in other systems that do not contain aluminum.[34−36]

In this work, we present results that show that during boehmite synthesis, in the initial stage, atoms array forming nanocapsules with shells made up of Al_{13} tridecamers; these

* Corresponding author. E-mail: bokhimi@fisica.unam.mx.
† The National University of Mexico.
‡ Universidad Autónoma Metropolitana-Iztapalapa.
§ Instituto Mexicano del Petróleo.

10.1021/jp053763n CCC: $30.25
Published on Web 11/08/2005

shells will be eventually transformed into boehmite. At room temperature, this transformation first requires the interaction between the nanocapsules to put in contact the atoms of the interacting shells.

The interaction between capsules opened the curved structure of their shells and created conditions for the rearrangement of the noncrystalline atom distribution, which, after aging the gel at room temperature for several days by evaporating the solvent, started to transform into a crystalline one that gave rise to thin crystalline boehmite bars, which ordered to gave rise to boehmite rods.

Experimental Section

Synthesis. Aluminum tri-*sec*-butoxide (Aldrich 97%) was dissolved and refluxed in anhydrous 2-propanol for 1 h at 85 °C; then, the hydrolysis catalyst, H_2SO_4, was added dropwise into the solution, continuing the refluxing for one more hour. Thereafter, the solution was cooled to room temperature, where the water was dropwise added, and the mixture was maintained at this temperature for 1 h; then, the temperature was raised to 85 °C and maintained there for 3 h. The molar ratios of the solution components were as follows: 2-propanol/AB = 60, H_2SO_4/AB = 0.03, and H_2O/AB = 1. The obtained sol was aged at room temperature for several days by just depositing it in a open glass vessel; the corresponding aged and nonaged products were dried overnight in static air at 120 °C; the dried solids were calcined from room temperature up to 700 °C at 4°/min, and maintained there during 4 h.

Experimental Techniques. X-ray Powder Diffraction. The X-ray diffraction pattern of the samples was measured in a theta-theta Bruker D-8 Advance diffractometer with Cu Kα radiation and a graphite secondary beam monochromator. Diffraction intensity was measured between 3° and 110°, with a 2θ step of 0.02° and a counting time of 9 s per point. The boehmite crystalline structure was refined via the Rietveld method using Fullprof code.[37] The crystallite morphology was modeled with spherical harmonics;[38] the background was modeled with a polynomial function that in addition to the constant, linear, quadratic, and cubic terms in 2θ, also contained the terms $(1/2\theta)$ and $(1/2\theta)^2$.

Transmission Electron Microscopy (TEM). Samples were analyzed with transmission electron microscopy in a JEOL 100CX and a JEOL JEM-2010F microscope. Samples were dispersed in ethanol before placing them in the copper grid with Formvar support.

^{27}Al MAS NMR Measurements. ^{27}Al spectra of the samples were obtained by using a Bruker ASX 300 spectrometer operating at the resonance frequency of 78.21 MHz, with the sample spinning at 10 kHz in a zirconia rotor. Spectra were recorded using a $\pi/2$ pulse of 2 μs and a recycle time of 0.5 s; 1 M $AlCl_3$ solution was used as chemical-shift reference.

Texture. Specific surface areas and pore diameter distributions were obtained from nitrogen adsorption−desorption isotherms measured in a Micromeritics ASAP-2100 analyzer. The adsorption was carried out in situ after outgassing the sample at 400 °C during 4 h under a residual pressure of 10^{-5} Torr.

Results and Discussion

The transmission electron micrograph of the nonaged sample prepared from the fresh sol shows that the sample was made up of rings (Figure 1A). Because the image was formed with transmitted electrons, these apparent rings could correspond to real rings or to hollow spheres. To distinguish which of these two geometries was the real one, an isolated particle was analyzed via TEM (Figure 2A) and STEM (Figure 2B−D)

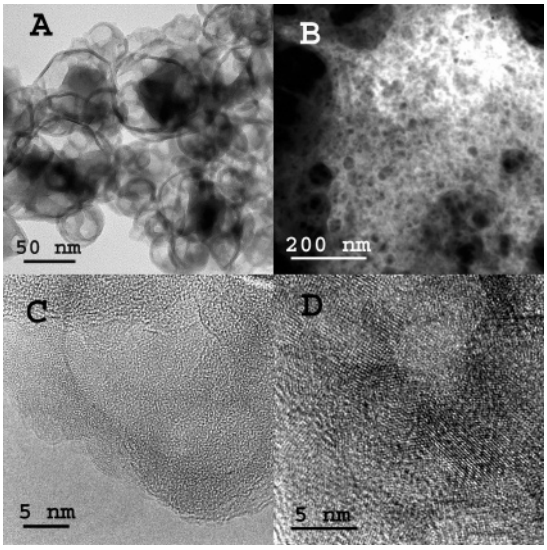

Figure 1. (A−C) TEM micrographs of the nonaged samples and (D) a sample aged for 20 days.

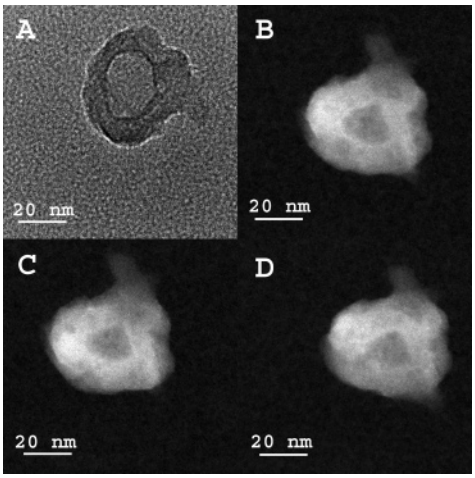

Figure 2. (A) TEM micrograph of an isolated capsule, (B) STEM micrograph of the same capsule, (C) STEM micrograph of the capsule after it was rotated +15° from its original position, and (D) STEM micrograph of the capsule after it was rotated −15° from its original position.

modes of the transmission electron microscope. After taking the image of the particle in its original position (Figure 2B), it was rotated +15° (Figure 2C) and −15° (Figure 2D) from this initial position, observing that the image was essentially the same for all the three different particle positions. This experiment clearly shows that the particles in the sample were hollow spheres (hereafter they will be identified as capsules) and not rings. These capsules were similar to those observed in the samples of polyelectrolyte templated on melamine formaldehyde and carbon cores,[39] and those observed in samples of hydrotalcite,[40] and in samples of Bi_2S_3.[41]

The capsules had an average diameter of 20 nm—the most frequently found diameters varied between 10 and 30 nm—and a shell thickness of 3.5 nm; the inner diameter of the capsule was similar to the observed average pore diameter (15.3 nm) when the sample was calcined at 700 °C (Table 1).

For the synthesis conditions used in the present work, in the nonaged sample, the capsules aggregated to generate a foam (Figure 1B). This aggregation morphology was specific for the present synthesis conditions, because recent experiments in our laboratory show that the capsules aggregation morphology depends on the synthesis temperature, the solute concentration,

TABLE 1: Sample Texture after Its Calcining at 700 °C

sample	average pore diameter (nm)	BET surface area (m^2/g)	total pore volume (cm^3/g)
nonaged	15.3	250	0.77
aged for 20 days	10.5	400	1.33

and the adding of external molecules such as surfactants to the solution during the synthesis.

The X-ray diffraction pattern of the nonaged sample (Figure 3B) shows that it was neither crystalline nor amorphous; the pattern was more similar to the one produced by randomly oriented molecules,[42] which is characterized by a few broad peaks representative of the bond lengths in the molecule.

Since solutions of aluminum salts give rise to Al_{13} tridecamers[43] that have the Keggin structure,[31,44] with one Al−O tetrahedron at the tridecamer center surrounded by 12 Al−O octahedra (Figure 4), and the ^{27}Al MAS NMR spectrum of the nonaged samples showed that they had the above-mentioned Al−O symmetries (Figure 5A), it is valid to assume that these tridecamers were present in the samples and that their atomic distribution would be responsible of the observed X-ray diffraction pattern.

To model the atom distribution of the Al_{13} tridecamer, we used the atom positions given by Johansson[31] (Table 2), which were derived from the crystallographic analysis of a cubic crystal of $Na_2O{\cdot}13Al_2O_3{\cdot}8SeO_2{\cdot}74H_2O$ that has a lattice parameter of 1.80 nm and a unit cell with the symmetry described by space group $F43m$. The X-ray diffraction pattern of the Al_{13} tridecamer with the above atom coordinates was calculated (Figure 3C) by using Debye's scattering equation for randomly oriented independent molecules[45]

$$I_{eu} = \sum_m \sum_n f_m f_n (\sin(kr_{mn})/kr_{mn})$$

I_{eu} is the scattering intensity in electron units; this unit corresponds to the classical X-ray scattering by a free electron. $\sum_m$ and $\sum_n$ represent the sum over all atoms in molecule; f_m and f_n are the atomic form factors; $k = (4\pi \sin\theta)/\lambda$, with θ the scattering angle and λ the X-ray wavelength; r_{mn} is the distance between atoms m and n.

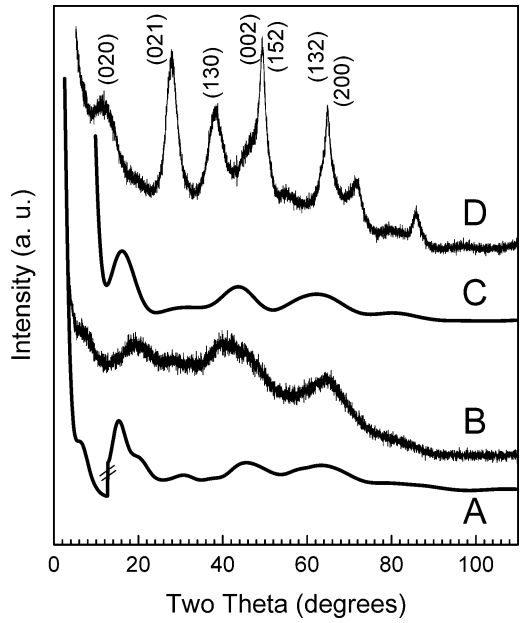

Figure 3. (B and D) Experimental X-ray powder diffraction pattern of the nonaged and aged samples, respectively; Miller indices correspond to boehmite. (C) Calculated X-ray diffraction pattern of randomly oriented noninteracting Al_{13} tridecamers. (A) Calculated pattern of randomly oriented clusters made up of five Al_{13} tridecamers interacting between each other; the intensities corresponding to the 2θ angles lower than 13° were divided by 20, to show all diffraction peaks in the same figure.

TABLE 2: Atom Positions in Al_{13} Tridecamer According to Johansson[a]

atom	site	x	y	z
Al1	48h	0.057	0.057	0.328
Al2	4b	0.500	0.500	0.500
O1	16e	0.441	0.441	0.441
O2	48h	0.047	0.047	0.677
O3	48h	0.158	0.158	0.447
O4	48h	0.069	0.069	0.223

[a] Ref 31.

Although the atom positions used for modeling the Al_{13} tridecamer corresponded to the atom positions of the tridecamer

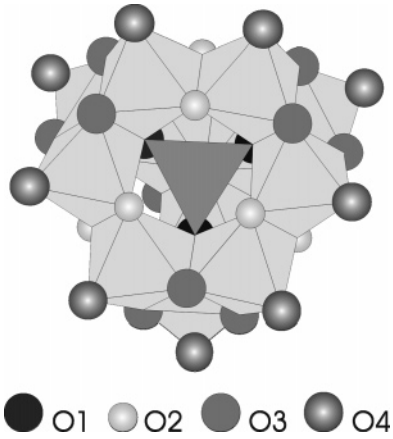

Figure 4. Atom distribution in the Al_{13} tridecamer.

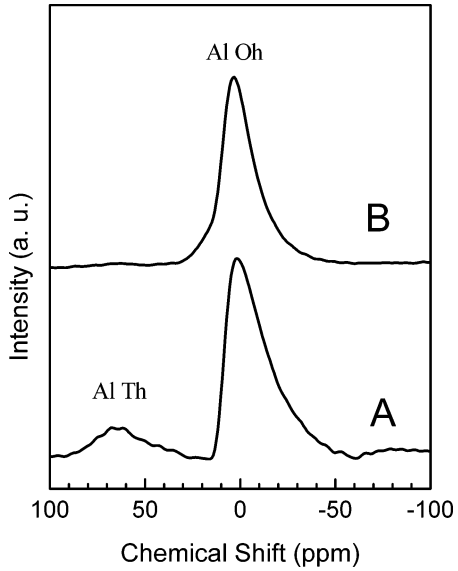

Figure 5. (A) ^{27}Al MAS NMR spectra of the nonaged sample and (B) of the sample aged for 20 days. Al Oh corresponds to aluminum atom in an octahedral environment; Al Th corresponds to aluminum atom in a tetrahedral environment.

forming part of a large crystallite of an aluminum selenide,[31] the calculated X-ray diffraction pattern reproduced, in a good approximation, the five broad peaks of the experimental pattern observed for angles above $2\theta = 12°$ (Figure 3C). The differences in the peak positions between the experimental and calculated diffraction patterns indicate that the atom positions of the Al_{13} tridecamers in the sample with the capsules were slightly shifted from the positions given by Johansson for the aluminum selenide.[31] The essence of the above comparison, however, was to show that the nanocapsules in the sample had a shell made up of Al_{13} tridecamers.

It must be remarked that the experimental X-ray diffraction pattern also contains a background produced by the scattering generated by the small finite size of the nanocapsules, which could be well approximated with the function $C1(2\theta)^{-1} + C2(2\theta)^{-2}$; C1 and C2 were fitting parameters. This function was also used successfully to model the background produced by the aged samples containing crystalline boehmite, which implies that the change in atomic local order did not change significantly the particle dimensions.

The model of randomly oriented independent Al_{13} tridecamers did not reproduce the first peak of the experimental X-ray diffraction pattern (Figures 3B and 3C), which corresponded to atom distances larger than those found in the Al_{13} tridecamer; therefore, we constructed a new model that considered the interaction between Al_{13} tridecamers.

In the literature there are several reports about the possible interactions between tridecamers with the Keggin structure.[34−36,46−48] Based on them, we constructed a very simple model where a central Al_{13} tridecamer interacts with other four Al_{13} tridecamers via the most external oxygen atoms,[48] O4 (Figure 4). Each one of these oxygen atoms was shared by two octahedra belonging to two different Al_{13} tridecamers. This atom rearrangement permits the distribution of electrons between the oxygen O4, O3, and O2 and the corresponding aluminum atoms at the octahedra center, instead of the characteristic cation behavior of the Al_{13} tridecamer when it is in a solution[43] or in an ionic crystalline structure.[31] To obtain an energetically stable atomic distribution for this large cluster of five Al_{13} tridecamers, all the interactions between neighboring atoms were varied using the molecular mechanical force-field model MM2[49] available in Chem3D software[50] until an energy minimum was found. In the initial tridecamers orientation, before energy minimization, one axis of the tetrahedron of each one of the four external Al_{13} tridecamers was placed nearly parallel to one axis of the tetrahedron of the central Al_{13} tridecamer. The final large cluster of five tridecamers also had the tetrahedral symmetry characteristic of the Al_{13} tridecamer. After minimizing the energy, the obtained atom positions of the large cluster were used to calculate its X-ray diffraction pattern (Figure 3A).

The calculated X-ray diffraction pattern using this new model was characterized by a peak at nearly the same position as the first peak in the experimental X-ray diffraction pattern. To see all peaks in the same figure, for the angles 2θ lower than 13° the intensity of the calculated diffraction pattern was divided by a factor of 20, because in the theoretical X-ray diffraction pattern the intensity of this peak was larger than the intensity of the others. The above result does not show that this is the exact way that Al_{13} tridecamers were ordered in the capsule's shell, but only that in the sample the Al_{13} tridecamers were ordered with neighboring distances similar to those obtained in the large cluster made of Al_{13} tridecamers described above; this ordering does not have the translational symmetry characteristic of a crystalline structure.

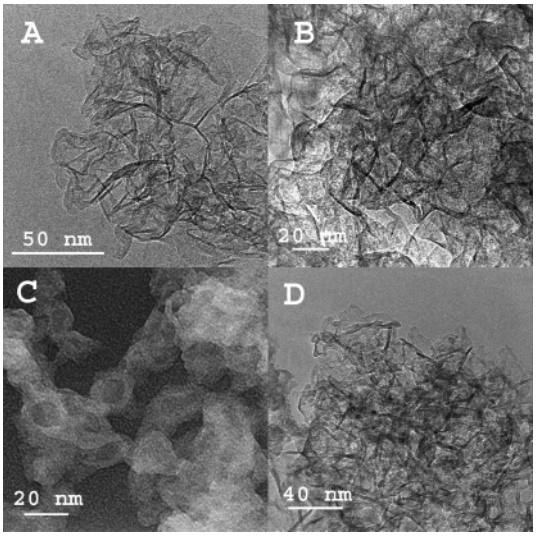

Figure 6. Micrographs of aged samples: (A) aged for a few days; (B) aged for 20 days. Micrographs of samples calcined at 700 °C: (C) a nonaged sample; (D) a sample aged for 20 days.

It is interesting to note that the diameter of the large cluster modeled above was about 4.0 nm, which is very similar to the capsule's shell thickness found experimentally. Besides, it must be remarked that the high-resolution image in the micrographs of the capsules (Figure 1C) shows that capsule's shell is rough with rounded protuberances, which could be associated to the atom distribution in the Al_{13} tridecamers.

The capsule's aggregation or coalescence caused the opening of the capsule's closed structure. The shell regions of neighboring interacting capsules produced a contrast in the micrograph that look like curved fibers (Figure 6A), with the same atomic local atom distribution present in the shell before the interaction, because the corresponding X-ray diffraction pattern was similar to the one shown in Figure 3B. The interaction between capsules depended on the number of sulfate ions in solution during the synthesis, because these ions interacted with the capsules surface, weakening the interaction between capsules.[51]

When the sample with the interacting capsules was aged at room temperature for several days, the atoms in the shell regions in contact rearranged from the local order of Al_{13} tridecamers into the one of the crystalline structure of boehmite (Figures 1D and 3D) made of only Al−O octahedra; therefore, the corresponding ^{27}Al MAS NMR spectrum did not have any more the peak corresponding to the Al−O tetrahedra (Figure 5B), but only the one corresponding to the Al−O octahedra. When the X-ray diffraction patterns of aged samples prepared with different H_2SO_4/AB molar ratios is analyzed,[51] it is evident that capsule's interaction decreases as this molar ratio increases (Figure 7); when this ratio was 0.09 no reflection of crystalline boehmite was observed, indicating that all capsules were covered with sulfate ions.

The change in atomic ordering during aging transformed the curved fibers (6A) into rods (Figure 6B), which is a particle morphology compatible with translational symmetry. Because the rods were crystalline, their structure was refined modeling the crystallite anisotropy with spherical harmonics in order to get details about the crystallite morphology: The refinement reveled that the rods were made of crystalline bars that had a nonsymmetrical eight-sided cross section, with their smallest dimension (1.21 nm) along the *b* axis, and their length along [001] or [100] directions. The crystalline bars growing along the [001] direction had an average length of 3.7 nm, while those growing along the [100] direction had a length of 2.2 nm.

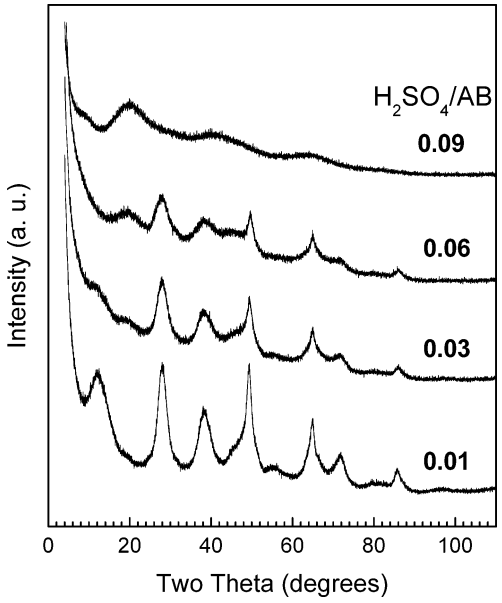

Figure 7. X-ray diffraction patterns of samples prepared with H_2SO_4/AB molar ratios between 0.01 and 0.09 and aged at room temperature for 30 days.

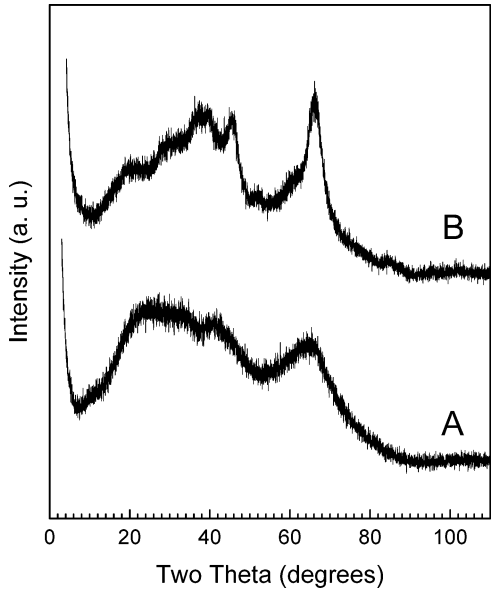

Figure 8. X-ray diffraction patterns of samples calcined at 700 °C: (A) a nonaged sample; (B) a sample aged for 20 days.

It is necessary to remark that the above dimensions correspond to domain regions where atoms are arranged in a crystalline symmetry, which are not necessarily equal to the rod dimensions observed in the micrographs: The rods in the micrographs had their smallest dimension similar to the one of the shell thickness, 3.5 nm, and lengths larger than 20 nm.

The dimensions of the crystalline bars obtained from the Rietveld refinement, which were about 3 times smaller along the cross section and 10 times smaller along their length axis than those of the rods observed in the micrographs, suggest that the rods were made of many thin crystalline bars stacked along the rod axis. The above rods made of crystalline bars are probably the precursors of the boehmite rods reported in the literature with a cross section of 2−4 nm and a length of 20−100 nm.[15−20]

It is important to note that the above-reported crystallization is related to the initial stage of boehmite crystallites formation when the precursor solution contains Al_{13} tridecamers. In the present case, the crystallization occurred after the capsules interacted between each other; therefore, solutions with a larger concentration of solute would produce more capsules which increases the probability of interaction and consequently the generation of more crystalline regions. Thereon, boehmite crystallization can be increased by controlling the capsule's aggregation; for example, by changing the OH/Al ion ratio in the solution using external hydrolyzing agents, such as sodium hydroxide,[31,52] sodium carbonate,[43,53] or ammonium hydroxide.[31,54] On the contrary, the capsule's aggregation can be decreased by adding ions or molecules in the solution that can cover the capsule's shell; for example, by increasing the amount of sulfate ions in the sample (Figure 7)[51] or by mixing the sample with nitric acid, which is frequently used to peptize colloidal dispersions.[55]

The initial roughness of capsule's shell surface observed in the nonaged samples did not change even after the opening and crystallization of the capsules through their interaction; therefore, the formed crystallites of boehmite also had a rough surface, as was evident when the crystallites edge was observed.

It is important to remark that the texture of the samples did not change when they were annealed at 700 °C (Figure 6C for the nonaged sample and Figure 6D for the aged one): the capsules morphology in the nonaged sample, and the fiber morphology in the aged samples, was conserved after the annealing. At this temperature the atom distribution in the nonaged sample, which was based on the one of the Al_{13} tridecamers, was transformed into the local order of a noncrystalline alumina phase (Figure 8A), and the one of boehmite was transformed into γ-alumina (Figure 8B).

The conservation of the particle morphology, and consequently the texture, in the aged samples is a well-known behavior in samples made up of boehmite[56,57] and is a consequence of the fact that the transformation of boehmite into γ-alumina is pseudomorphic.

In the nonaged samples, however, the conservation of the capsule's morphology is a new result, which suggests that the transformation of the phase made up of Al_{13} tridecamers into the noncrystalline alumina phase was also pseudomorphic.

The results described above clearly show that, when solutions of aluminum compounds are prepared, a morphology of nanocapsules with shells made up of Al_{13} tridecamers is the atomic ordering that follows the formation of the polynuclear Al_{13} tridecamers and that the interaction between capsules generates the conditions to produce an atom distribution with translational symmetry, which eventually gives rise to crystalline bars of boehmite. The above sequence of atomic ordering is not necessarily the only one that exists in nature when aluminum salts are dissolved. Many other atomic ordering sequences may be possible, depending of the synthesis conditions; to find them, however, requires a systematic work during the synthesis and a detailed analysis of the atomic local order evolution.

It is interesting to mention that the opening of the capsules through their interaction increased the specific surface area and the pore volume of the material (Table 1), as obtained from the nitrogen adsorption−desorption experiments of the samples calcined at 700 °C. The specific surface area and the total pore volume of the samples increased from 250 m^2/g and 0.77 cm^3/g for the nonaged sample to 400 m^2/g and 1.33 cm^3/g for the aged one. To test the stability of the texture we also measured the above parameter after calcining the sample at 550 °C, obtaining values similar to those observed in the sample calcined at 700 °C.

The above results are of much interest in catalysis, either when alumina is used as a support or when it is the active phase of the catalyst.

Conclusions

By using the sol−gel method with aluminum tri-*sec*-butoxide as aluminum precursor and 2-propanol as solvent, nanocapsules with shells made up of Al_{13} tridecamers were obtained with an average diameter of 20 nm and a shell thickness of 3.5 nm. The X-ray diffraction characterization of the capsules shells shows that the Al_{13} tridecamers in the shell were not independent from each other; they were ordered in a noncrystalline structure. When the nanocapsules aggregated or coalesced, the interaction between shells of neighboring capsules caused the opening of the capsule's morphology, which, when the sample was aged at room temperature, favored the transformation of the Al_{13} tridecamer atomic distribution into a crystalline atomic order that eventually gives rise to nanocrystalline bars of boehmite. This capsule opening increased the pore volume and the specific surface area of the sample. Nanocapsule morphology was preserved after calcining the sample at 700 °C, indicating that the transformation of the capsules shell made up of ordered Al_{13} tridecamers into a noncrystalline alumina was pseudomorphic. The sequence of phase transformations shows a possible evolution of the atom distribution when solutions of aluminum compounds are prepared: this evolution starts with the formation of Al_{13} tridecamers, which interact between each other ordering and forming nanocapsules; then, these nanocapsules interacted between each other opening their capsule structure and favoring the transformation of the atomic local order of Al_{13} tridecamers into the one of boehmite which gives rise to a crystalline ordering.

Acknowledgment. We thank Dr. Juan Rodriguez-Carbajal, LLB, France, for allowing us to use the library of the CrysFML software package that contains the parameters to calculate the atomic form factors. We thank M. Sc. Manuel Aguilar, Mr. Antonio Morales, and Mr. L. Rendón for technical assistance, and the IMP-Molecular Engineering Research Program for financial support of the Project D.00285.

References and Notes

(1) Ertl, G.; Knözinger, H.; Weitkamp, J. *The Handbook of Heterogeneous Catalysis*; Wiley-VCH: Weinheim, Germany, 1997.
(2) Misra, C. *Industrial Alumina Chemicals*; ACS Monograph 184; American Chemical Society: Washington, DC, 1986.
(3) Hellgardt, K.; Chadwick, D. *Ind. Eng. Chem. Res.* **1998**, *37*, 405.
(4) Knözinger, H.; Ratnasamy, P. *Catal. Rev.—Sci. Eng.* **1978**, *17*, 31.
(5) Lippens, B. C. Structure and Texture of Aluminas. Ph.D. Thesis, Technical University of Delft, Amsterdam, 1961.
(6) Ono, T.; Ohguchi, Y.; Togari, O. In *Preparation of Catalysts III*; Poncelet, G., Grange, P., Jacobs P. A., Eds.; Elsevier: Amsterdam, 1983; p 631.
(7) Trimm, D. L.; Stanislaus, A. *Appl. Catal.* **1986**, *21*, 215.
(8) Mishra, D.; Anand, S.; Panda, R. K.; Das, R. P. *Mater. Lett.* **2000**, *42*, 38.
(9) Tsuchida, T. *J. Eur. Ceram. Soc.* **2000**, *20*, 1759.
(10) Vaudry, F.; Khodabandeh, S.; Davis, M. E. *Chem. Mater.* **1996**, *8*, 1451.
(11) Krokidis, K.; Raybaud, P.; Gobichon, A.-E.; Rebours, B.; Euzen, P.; Toulhoat, H. *J. Phys. Chem. B* **2001**, *105*, 5121.
(12) Ttemuijin, J.; Jadambaa, T. S.; Mackenzie, K. J. D.; Angerer, P.; Porte, F.; Riley F. *Bull. Mater. Sci.* **2000**, *23*, 301.
(13) Chuah, G.; Jaenicke, S.; Xu, T. H. *Microporous Mesoporous Mater.* **2000**, *37*, 345.
(14) Lippens, B. C.; de Boer, J. H. *Acta Crystallogr.* **1964**, *17*, 1312.
(15) Zhang, Z.; Pinnavaia, T. J. *J. Am. Chem. Soc.* **2002**, *124*, 12294.
(16) Lee, H. C.; Kim, H. J.; Chung, S. H.; Lee, K. H.; Lee, H. C.; Lee, J. S *J. Am. Chem. Soc.* **2003**, *125*, 2882.
(17) Ram, S.; Singh, T. B.; Pathak, L. C. *Phys. Status Solidi A* **1998**, *165*, 151.
(18) Wierenga, A.; Philipse, A. P.; Lekkerkerker, H. N. W.; Boger, D. V. *Langmuir* **1998**, *14*, 55.
(19) Zhu, H. Y.; Riches, J.; Barry, J. C. *Chem. Mater.* **2002**, *14*, 2086.
(20) Zhu, H. Y.; Gao, X. P.; Song, D. Y.; Bai, Y. Q.; Ringer, S. P.; Gao, Z.; Xi, Y. X.; Martens, W.; Riches, J. D.; Frest, R. L. *J. Phys. Chem. B* **2004**, *108*, 4245.
(21) Buining, P. A.; Pathmamanoharan, C.; Jansen, J. B. H.; Lekkerkerker, H. N. W. *J. Am. Ceram. Soc.* **1991**, *74*, 1303.
(22) Maki, T.; Sakka, S. *J. Non-Cryst. Solids* **1988**, *100*, 303.
(23) Noweck, K. *Alumina Brochure*; Condea Chemie: Hamburg, Germany, 2000.
(24) González-Peña, V.; Díaz, I.; Márquez-Álvarez, C.; Sastre, E.; Pérez-Pariente, J. *Microporous Mesoporous Mater.* **2001**, *44*−*45*, 203.
(25) Buining, P. A.; Pathmamanoharan, C.; Bosboom, M.; Jansen, J. B. H.; Lekkerkerker, H. N. W. *J. Am. Ceram. Soc.* **1990**, *73*, 2385.
(26) Bokhimi, X.; Toledo-Antonio, J. A.; Guzmán-Castillo, M. L.; Mar-Mar, B.; Hernández-Beltrán, F.; Navarrete, J. *J. Solid State Chem.* **2001**, *161*, 319.
(27) Dragcevic, D.; Popovic, S. *Mater. Lett.* **1999**, *40*, 269.
(28) Bokhimi, X.; Toledo-Antonio, J. A.; Guzmán-Castillo, L. M.; Hernández-Beltrán, F. *J. Solid State Chem.* **2001**, *159*, 32.
(29) Vázquez, A.; López, T.; Gómez, R.; Bokhimi Morales, A.; Novaro, O. *J. Solid State Chem.* **1997**, *128*, 161.
(30) Martens, W. N.; Frost, R. L.; Bartlett, J.; Kloprogge, J. T. *J. Mater. Chem.* **2001**, *11*, 1681.
(31) Johansson, G. *Acta Chem. Scand.* **1960**, *14*, 771.
(32) Singhal, A.; Keefer, K. D. *J. Mater. Res.* **1994**, *9*, 1973.
(33) Vogels, R. J. M. J.; Kloprogge, J. T.; Buining, P. A.; Seykens, D.; Jansen, J. B. H.; Geus, J. W. *J. Non-Cryst. Solids* **1995**, *191*, 38.
(34) Nyman, M.; Bonhomme, F.; Alam, T. M.; Rodriguez, M. A.; Cherry, B. R.; Krumhansl, J. L.; Nenoff, T. M.; Sattler, A. M. *Science* **2002**, *297*, 996.
(35) Kang, Y.; Li, M.; Zhao, J.; Mao, S. *Acta Crystallogr., Sect. E* **2004**, *60*, i97.
(36) Xu, Y.; Xu, J.-Q.; Yang, G.-Y.; Yang, G.-D.; Xing, Y.; Lin, Y.-H.; Jia, H.-Q. *Acta Crystallogr., Sect. C* **1998**, *54*, 9.
(37) Rodriguez-Carbajal, J. Laboratoire Leon Brilloin (CEA-CNRS), France; e-mail juan@llb.saclay.cea.fr.
(38) Kara, M.; Kurki-Suonio, K. *Acta Crystallogr., Sect. A* **1981**, *37*, 201.
(39) Sukhorukov, G. B.; Shchukin, D. G.; Dong, W.-F.; Moehwald, H.; Lulevich, V. V.; Vinogradova, O. I. *Mol. Chem. Phys.* **2004**, *205*, 530.
(40) Valente, J.; Bokhimi, X. To be submitted for publication.
(41) Vega-González, M.; Bokhimi, X. To be submitted for publication.
(42) Warren, B. E. *X-ray Diffraction*; Addison-Wesley: Reading, MA, 1969; p 116.
(43) Rausch, W. V.; Bale, H. D. *J. Chem. Phys.* **1964**, *40*, 3391.
(44) Allouche, L.; GeÂrardin, C.; Loiseau, T.; FeÂrey, G.; Taulelle, F. *Angew. Chem., Int. Ed.* **2000**, *39*, 511.
(45) Debye, P. *Ann. Phys.* **1915**, *46*, 809.
(46) Almeida-Paz, F. A.; Sousa, F. P.; Soares-Santos, P. C. R.; Cavaleiro, A. M. V.; Nogueira, H. I. S.; Klinowski, J.; Trindade, T. *Acta Crystallogr., Sect. E* **2004**, *60*, m1.
(47) Weng-Ng, S. *Acta Crystallogr., Sect. E* **2004**, *60*, m1786.
(48) Sugeta, M.; Yamase, T. *Acta Crystallogr., Sect. C* **1997**, *53*, 1166.
(49) Allinger, N. L. *J. Am. Chem. Soc.* **1977**, *99*, 8127.
(50) *ChemBats3D Ultra 9.0*; Cambridgesoft Corporation: Cambridge, MA, 2005; http://www.cambridgesof.com/.
(51) Bokhimi, X.; Sánchez-Valente, J. To be submitted for publication.
(52) Schaefer, D. W.; Shelleman, R. A.; Keefer, K. D.; Martin, J. E. *Physica A* **1986**, *140A*, 105.
(53) Ruff, J. K.; Tyree, S. Y. *J. Am. Chem. Soc.* **1958**, *80*, 1523.
(54) Bale, H. D.; Schmidt, P. W. *J. Chem. Phys.* **1959**, *31*, 1612.
(55) Pottier, A.; Chaneac, C.; Tronc, E.; Mazerolle, L.; Jolivet, J.-P. *J. Mater. Chem.* **2001**, *11*, 1116.
(56) Sánchez-Valente, J.; Bokhimi, X.; Hernández, J.; Guzman-Castillo, M. L.; Fripiart, J. J. *J. Mater. Res.* **2004**, *19*, 1499.
(57) Tikhov, S. F.; Fenelonov, V. B.; Zaikovskii, V. I.; Potapova, Yu. V.; Sadykov, V. A. *Microporous Mesoporous Mater.* **1999**, *33*, 137.